Hindawi
Shock and Vibration
Volume 2021, Article ID 9246947, 15 pages
https://doi.org/10.1155/2021/9246947

Research Article

Discrete Simulation of Vibratory Roller Compaction of Field Rockfills

Yang Li and Chengxue She

State Key Laboratory of Water Resources and Hydropower Engineering Science, Wuhan University, Wuhan 430072, China

Correspondence should be addressed to Chengxue She; cxshe_whuslsd@whu.edu.cn

Received 4 November 2019; Revised 13 January 2021; Accepted 4 February 2021; Published 2 March 2021

Academic Editor: Xavier Chiementin

Vibratory roller compaction is a well-known method in improving the mechanical properties of field rockfills. However, the meso mechanism of rockfill densification under vibratory roller compaction has not been understood clearly. This paper presents a discrete numerical method to simulate the vibratory roller compaction of field rockfills. Firstly, rockfill particles were modeled by irregular and stochastic clusters, which can be breakable. In addition, the segregation of field rockfills was replicated in a practical manner. Then, a new model of the vibratory roller was presented, in which the frame inertia was considered. Finally, the developed method was applied to simulate the vibratory roller compaction of field rockfills in the Shui Buya Project. Results show that (1) the numerical simulations of vibratory roller compaction of field rockfills agree well with the field experiments; thus, the feasibility and rationality of the developed simulation method are verified; (2) the dynamic response of field rockfills under vibratory roller compaction can be predicted by the presented numerical method with calibrated model and parameters; (3) the new roller model with frame inertia considered is much more accurate than the roller models in early studies. Thus, the developed discrete numerical method can be further adopted to explore the meso mechanism of rockfill densification under vibratory roller compaction in the future.

1. Introduction

Concrete-Faced Rockfill Dams (CFRDs) have been a popular dam type in hydropower engineering throughout the world since they are characterized by favorable adaptability of the dam foundation, full utilization of local materials and building-excavated materials, low construction cost, and low cement consumption [1, 2]. CFRDs are currently being developed from a 200 m high level to a 300 m high level in China [3]. Large dam height can lead to poor performance, such as large settlements, severe cracking, and excessive leakage [4]. Thus, it is more urgent than ever to ensure the safe and stable operation of high CFRDs.

The safe and stable operation of high CFRDs are closely dependent on the mechanical properties of field rockfills. Nowadays, vibratory roller compaction has been a well-known and widespread method to improve the mechanical properties of rockfills [5]. During the vibratory roller compaction of field rockfills (see Figure 1), rockfill particles are dumped from a truck, then a dozer with a raised blade pushes large rockfill particles ahead where the full thickness of pavement can accept them, and small rockfill particles fall under the blade, and then the rockfill pavement is compacted by a vibratory roller for several passes. As a benefit from the vibratory roller compaction technique, the post-settlements of modern CFRDs are much less than those of dumped CFRDs in the early years [5].

The compaction quality of field rockfill under vibratory roller compaction depends closely on the compaction parameters, such as roller mass, excitation force magnitude, frequency, roller passes, and pavement thickness (Zhong et al.) [6]. However, these parameters are usually determined by experience or field experiments rather than by theories [3, 5], and the reason is that the dynamic behavior of field rockfills under vibratory roller compaction has not been explored systematically yet. A better understanding of the

Figure 1: Vibratory roller compaction of field rockfills.

dynamic response of rockfills under vibratory roller compaction will help control the compaction quality effectively and economically and, more importantly, provide scientific support for the design and construction of high CFRDs. Thus, it is of great significance to study the vibratory roller compaction of field rockfills.

Field experiments are the usual approach to investigate the dynamic response of rockfills during vibratory roller compaction. For example, Zhu et al. [7, 8] conducted a series of field experiments of rockfill compaction to study the filling standard of high rockfill dams. An et al. [9] performed field experiments of rockfill compaction with various roller speeds and frequencies to optimize compaction parameters. Except for that, full-scale experimental investigations were also performed to explore the vibratory roller compaction on soil [10–12], asphalts [13], crushed gravel [14, 15], and concrete [16]. However, field experiments of granular materials are always costly and time-consuming. Moreover, experimental exploration can only reveal the dynamic response of granular material under vibratory roller compaction on the macroscopic scale, while the meso mechanism of the densification of granular material is still challenging to be thoroughly investigated.

Except for the experimental approach, numerical simulation has also been an alternative method to study the vibratory roller compaction of granular materials. Today, it is possible to model the vibratory roller compaction of soil using finite-element method [17]. However, to accurately predict the behavior of rockfill under vibratory roller compaction, it is necessary to model the relative motion of individual particles. This object can be realized by the discrete element method (DEM) proposed by Cundall and Strack [18]. Discrete modeling of rockfill material has been a hot topic since the last few years, and numerous efforts were made to explore the macro- and meso-behavior of rockfill material by DEM [19–21]. However, almost all these researches are focused on the behaviors of scaled rockfill samples in lab, which are different from the prototype field rockfills. For example, rockfill particles with various sizes were usually assumed to be distributed uniformly in the scaled samples in lab, while this assumption is no longer valid for the prototype field rockfill since rockfill particles at field are usually segregated [5].

Owing to the novelty of DEM and its difficulties, including long-time calculation, there is a lack of studies on DEM simulation of the vibratory roller compaction of field rockfills [14]. Liu et al. [22] made an effort to simulate the entire compaction process of rockfill in situ using DEM and replicated the irregular particle shape of rockfill grains using laser scanning technology. However, the rockfill particles in their work were assumed to be rigid, and breakage behavior of rockfill particles was ignored. Particle breakage has already been recognized as one of the critical factors that influence the mechanical behavior of rockfill [23]; thus, it will be improper to model rockfill material without considering the particle breakage. As a result, it is necessary to develop a more accurate discrete model for field rockfills, considering the particle segregation and breakage behavior.

When modeling the vibratory roller compaction of rockfill materials, it should also replicate the vibratory roller as true as possible. Among the present investigations on vibratory roller compaction of granular materials, the vibratory roller was usually modeled as a rigid plate [24, 25], or single drum [17, 22, 26], in which the frame inertia was always ignored due to the assumption that any effect on the drum due to the frame inertia was negligible. However, Mooney and Rinehart [12] have emphasized that this assumption is satisfactory for single drum roller, where the ratio of the drum to the frame mass is typically between 1.5 and 2, but it is less valid for tandem rollers, where the ratio of the drum mass to the frame mass can be lower. Thus, it is necessary to develop a more accurate numerical model for the vibratory roller.

The purpose of this paper is to develop a numerical method to simulate the vibratory roller compaction of field rockfills using DEM and verify the feasibility and rationality of developed method. The software used in this paper is PFC^{2D} released by ITASCA [27]. The major innovation of this paper is that the vibratory roller compaction of field rockfill is realized based on DEM successfully, overcoming the inherent difficulties of DEM modeling and long-time calculation. The achievements adopted in this paper can be adopted to explore the dynamic response of field rockfill under vibratory roller compaction in mesoscale, which enables a better understanding of the mechanical mechanism of rockfill densification. The remainder of this paper was organized as follows. Firstly, the modeling procedure of field rockfill was introduced in detail, considering the shape and breakage behavior of rockfill particles, and the segregation of the rockfill pavement. Then, a new numerical model of the vibratory roller was presented, in which the frame inertia was involved. At last, the presented numerical method was applied to simulate the vibratory roller compaction of field rockfills in the Shui Buya Project, and results of numerical simulation were compared with those of field experiments.

2. Discrete Modeling of Field Rockfill

2.1. Rockfill Particles considering Shape and Breakage. On the particle scale, the parameters that influence rockfill materials most are the shape and breakage of rockfill particles [19]. The shape of rockfill particle is usually irregular and stochastic. In recent years, significant efforts have been made to model realistic particle shape of rockfill particles by DEM [28–30].

To consider the effect of particle shape, convex polygonal particles from circles are generated to reflect the complex geometric features of rockfill particles in this paper (see Figure 2), which is similar to the method adopted by Zhou et al. [29]. According to the method, the position of all the polygonal vertices can be calculated as follows:

$$\begin{cases} x_k = x_c + R\cos\delta_k, \\ y_k = y_c + R\sin\delta_k, \end{cases} \quad (1 \le k \le N), \tag{1}$$

where (x_k, y_k) is the position of the kth vertice, (x_c, y_c) is the center of the circle, and R is the circle radius, N is the number of polygonal vertices, and δ_k is defined as follows,

$$\delta_k = \begin{cases} \alpha, & (k = 1), \\ \sum_{i=1}^{k-1} \theta_k, & (2 \le k \le N), \end{cases} \tag{2}$$

where α is the phase angle, which is chosen randomly in the range $(0, \pi/2)$, and θ_k is the angle corresponding to the kth edge, which is generated according to the following relationship,

$$\begin{cases} \beta_k = 2\pi\dfrac{[1 + (2b_k - 1)c]}{N}, \\ \theta_k = \beta_k\left(\dfrac{2\pi}{\sum_{i=1}^{N}\beta_i}\right), \\ (1 \le k \le N), \end{cases} \tag{3}$$

where b_k is a uniformly distributed number in the interval [0,1], and c is a constant parameter with absolute value less than 1.

After the shape is defined, a rigid particle is then created according to the geometry of the particle shape (see Figure 3(a)). Subsequently, the rigid particle is meshed into several triangle and rigid subparticles (Figure 3(b)). Then, cohesive and breakable bonds are installed at the contacts between neighboring subparticles (Figure 3(c)). When the bond fails, the breakage of the rockfill particle occurs. Thus, the breakage behavior of real rockfill particles can be replicated by this way.

It should be noted that the number of subparticles formulating the rockfill particle model determines the resolution of the model and has significant influences on the computation time for large-specimen DEM simulation [31]. As the purpose of this paper is to simulate the vibratory roller compaction of field rockfills, which is rather time-consuming, the number of subparticles that constitutes the rockfill particle model must be small to run simulations in reasonable time. Thus, 12–20 subparticles are adopted to form a rockfill particle model in this paper after a careful consideration.

2.2. Field Rockfill Pavement considering the Effect of Segregation. According to Cooke [5], rockfill pavement in situ is usually segregated, as shown in Figure 4. In the field rockfill pavement, coarse particles are usually in the bottom half, and fine particles are in the upper half mostly.

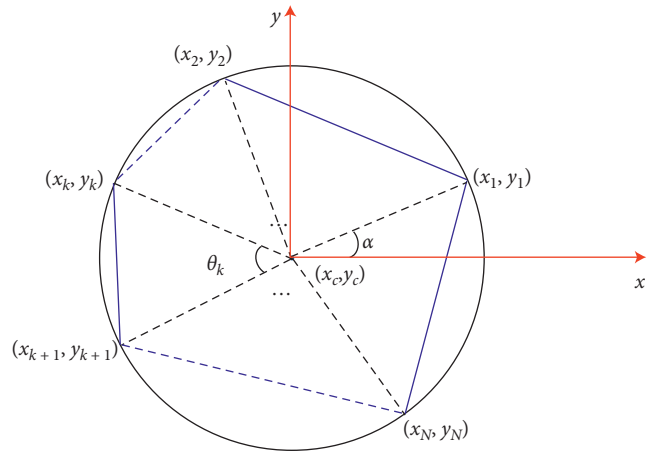

Figure 2: Definition of polygonal particle shape from circles.

This paper focuses on the effect of segregation, but not on the mechanism of how segregation occurs. In addition, to the best of our knowledge, the effect of segregation has not ever been considered in DEM models of field rockfills before. Thus, the DEM modeling of segregated rockfill pavement in this paper must be simplified to make the simulation possible. Based on this view, an appropriate but practical modeling procedure of the segregated rockfill pavement is presented in this paper, which is described as follows:

(1) Firstly, the largest rockfill particles with 400~800 mm in size are generated randomly in the model domain and dropped under gravity (Figure 5(a)).

(2) Then, the second-largest rockfill particles with 200~400 mm in size are generated randomly in the rest of the model domain, where it is not occupied by the largest particles (Figure 5(b)). Moreover, they are also dropped under gravity subsequently (Figure 5(c)).

(3) Steps (1) and (2) are repeated until all the rockfill particles are generated, and the model domain is filled with rockfill particles (Figure 5(d)).

According to Figure 5, it can be found in the DEM model of field rockfill pavement that coarse rockfill particles are distributed at the bottom of the pavement and fine particles at the top mostly, which is similar to the observation in the field rockfills. Thus, the segregation of rockfill pavement is replicated through the developed DEM modeling procedure qualitatively.

3. A New Numerical Model of Vibratory Roller with the Frame Inertial Considered

3.1. Fundamental Theory. Early efforts made by Yoo [32] proposed a 2-degree-of-freedom (DOF) model to represent steady-state vertical drum and frame kinematics. The general framework for the roller-soil model is illustrated in

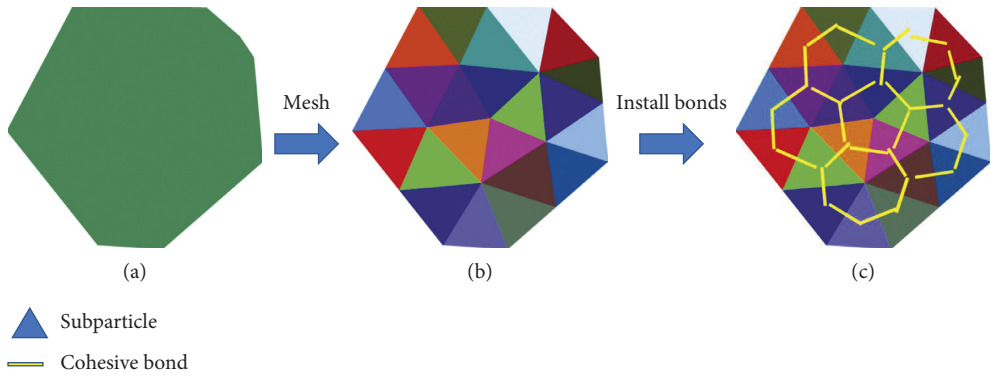

Figure 3: Modeling procedure of rockfill particles, considering the shape and breakage. (a) Polygon block; (b) assembly of subparticles; (c) breakable cluster.

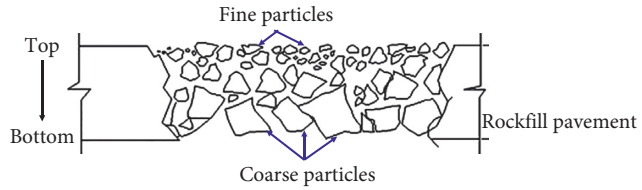

Figure 4: Segregation of field rockfill pavement (Modified from Cooke [5]).

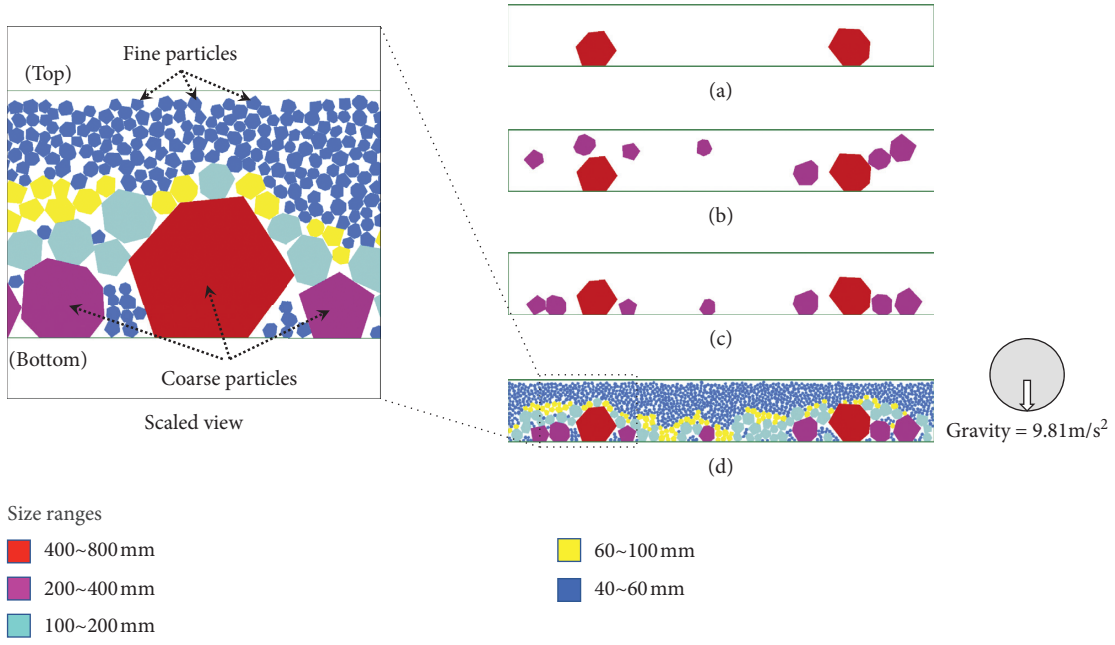

Figure 5: Modeling procedure of field rockfill pavement, considering the effect of segregation.

Figure 6, where the frame and drum are modeled with mass-spring-dashpot components.

The equations of motion for contact behavior (ignoring the drum-soil decoupling) are determined via force equilibrium using free body diagrams of frame and drum. And equations (4) and (5) represent drum and frame behavior during drum/soil contact mode vibration.

$$m_d\ddot{x}_d + c_{df}\left(\dot{x}_d - \dot{x}_f\right) + k_{df}\left(x_d - x_f\right) + c_{ds}\dot{x}_d + k_{ds}x_d - m_d g = F_{\max}\sin(2\pi f t), \tag{4}$$

$$m_f\ddot{x}_f + c_{df}\left(\dot{x}_f - \dot{x}_d\right) + k_{df}\left(x_f - x_d\right) - m_f g = 0, \tag{5}$$

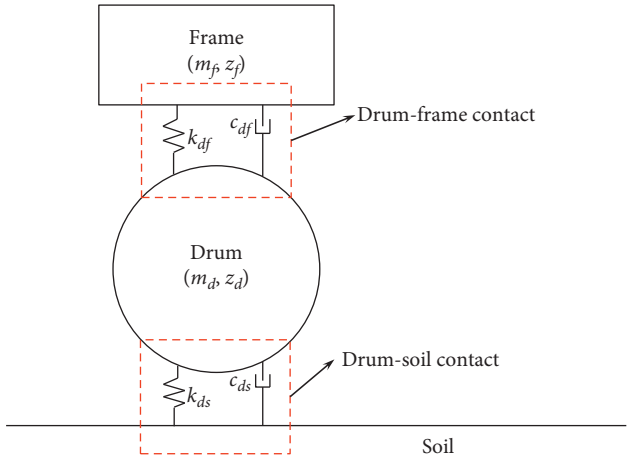

Figure 6: The 2DOF lumped parameter model of roller-soil system (Modified from Yoo [32]).

where m_d and m_f are mass of drum and frame, respectively. x_d and x_f are displacement of drum and frame, respectively, and superposed dot indicates time derivative. c_{df} is drum-frame damping, and k_{df} is drum-frame stiffness. c_{ds} is drum-soil damping, and k_{ds} is drum-soil stiffness.

The contact force F_c between the drum and soil can be determined from drum motion [see equation (6)].

$$F_c = k_{ds}x_d + c_{ds}\dot{x}_d. \tag{6}$$

For all equations, displacement, velocity, and acceleration are downward positive as shown in Figure 6. Zero displacement is defined as the location of the masses before any force (including gravity) is applied. Equations (4) and (5) can then be solved by finite difference numerical method.

3.2. New Model of Vibratory Roller. Inspired by the 2DOF model of vibratory roller proposed by Yoo [32], a new numerical model of vibratory roller was developed in this paper, which is illustrated in Figure 7. In the developed model of vibratory roller, the drum is modeled as a rigid cylindrical block with D_{drum} in diameter and m_d in mass, and the frame is also modeled as a rigid block with m_f in mass. The drum model contacts with the frame model, and no overlap exists between them initially. Linear contact bond model is installed at the contact between the drum and frame model, which contains three components, a linear spring with stiffness k_n, a cohesive bond with infinity strength, and a viscous dashpot with damping β_n. The contact between the drum and frame model can transfer force but no bending moment so that the drum can rotate freely.

Note that the k_n and β_n are meso parameters adopted in the roller model, and they can be calculated according to Ref [27],

$$k_n = k_{df},$$
$$\beta_n = \frac{c_{df}}{2\sqrt{m_d m_f k_n/\left(m_d + m_f\right)}}. \tag{7}$$

An external force F, which varies with time t, is applied to the drum model through a FISH script. The applied force F can be calculated as follows:

$$F = F_{\max}\sin\left(2\pi f t\right), \tag{8}$$

where $F_{\max}$ is the maximum excitation force, f is the vibration frequency, and t is time.

To model the traveling process, the roller model moves at a constant horizontal velocity v, and the drum rotates at a corresponding rotation speed w. The horizontal velocity v and rotation speed w satisfy the following relationship:

$$v = \frac{D_{\text{drum}}}{2}\omega. \tag{9}$$

3.3. Model Verification. In the roller model developed in this paper, the frame inertia is considered for the first time, which is the major innovation when compared to the roller models proposed in earlier studies [17, 22, 26]. To illustrate the effect of frame inertia, the classical problem of roller-soil compaction was resolved based on these two roller models, respectively. In the simulation, the roller lied on the top surface of the soil under gravity with equilibrium initially, and then it began to vibrate. To be specific, the type of roller was Sakai SV510D, and the soil was treated as a viscoelastic material. The typical properties of the roller and soil are summarized in Table 1. Moreover, the drum was assumed to contact the soil all the time, without considering the decoupling of roller and soil.

Numerical models for the roller-soil compaction are illustrated in Figure 8. In the numerical simulation, the Sakai SV510D roller was simulated by the new roller model with frame inertia considered (Figure 8(a)) and that in early studies without the frame inertia (Figure 8(b)), respectively. The soil was modeled through a rigid wall, and the deformation behavior of soil was represented by the overlap between the drum and wall. During the simulation, the displacements of the drum and frame model were recorded, as well as the contact force between the drum and soil. In addition, the analytical results for this soil-roller problem can be obtained by employing the finite difference method to solve equations (4) and (5).

Figure 9 illustrates the displacements of the drum and frame model. And Figure 10 displays the contact forces between the drum and soil. It can be found that the results based on the new model of roller in this paper are in good agreement with analytical solutions. However, the results based on the roller model in early studies have evident deviations. Notably, the contact force of the drum applied to the soil in this paper is much more accurate than that of the early studies. Thus, the new roller model is preferable when simulating the vibratory roller compaction of field rockfills.

4. Discrete Simulation of Vibratory Roller Compaction of Field Rockfills: A Case Study

In this part, a case study of the vibratory roller compaction of field rockfills in the Shui Buya Project was performed based

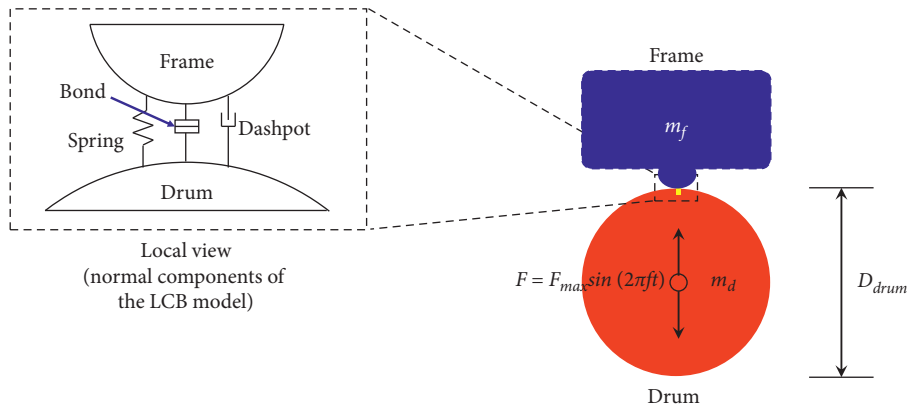

Figure 7: The developed numerical model of vibratory roller.

Table 1: Sakai SV510D Roller and soil parameters.

Parameter	Value	
Sakai SV510D roller	Drum mass, m_d (kg)	4466
	Frame mass, m_f (kg)	2534
	Excitation force, $F_{\max}$ (kN)	108
	Excitation frequency, f (Hz)	30
	Drum/frame stiffness, k_{df} (MN/m)	6.02
	Drum/frame damping, c_{df} (kg/s)	4000
Soil	Drum/soil stiffness, k_{ds} (MN/m)	8.00
	Drum/soil damping, c_{ds} (kg/s)	2000

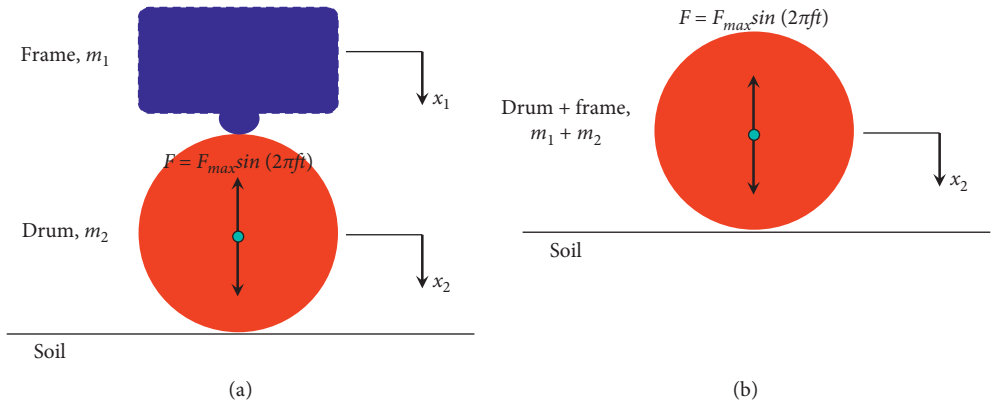

Figure 8: Numerical models for the soil-roller compaction. (a) The roller model in this paper; (b) the roller model in early studies [17, 22, 26].

on the developed modeling method, and results of the numerical simulations were compared with those of the experiments in detail.

4.1. Introduction of Field Experiments. The Shui Buya rockfill dam with a height of 233 m is the highest CFRD in the world at the present time. Before the formal construction of the dam body, a series of vibratory roller compaction experiments of the field rockfills were performed, and sufficient experimental data were recorded [33]. Rockfill materials used in the field experiments came from quarry blasted limestone, whose particle shape was angular. A brief introduction of the field experiments is summarized in Table 2.

Vibratory rollers adopted in the field experiments were the YZT16 roller and YZT18 roller. The terms YZT16 and YZT18 represent the type, or the name, of these rollers, respectively. And the specific properties of these two rollers are listed in Table 3.

The maximum particle size of rockfill in situ is 800 mm, and the minimum is 1 mm. The particle size distribution (PSD) of the field rockfill particles is presented in Figure 11.

In this paper, we have investigated three cases of the field experiments, of which various roller types and lift

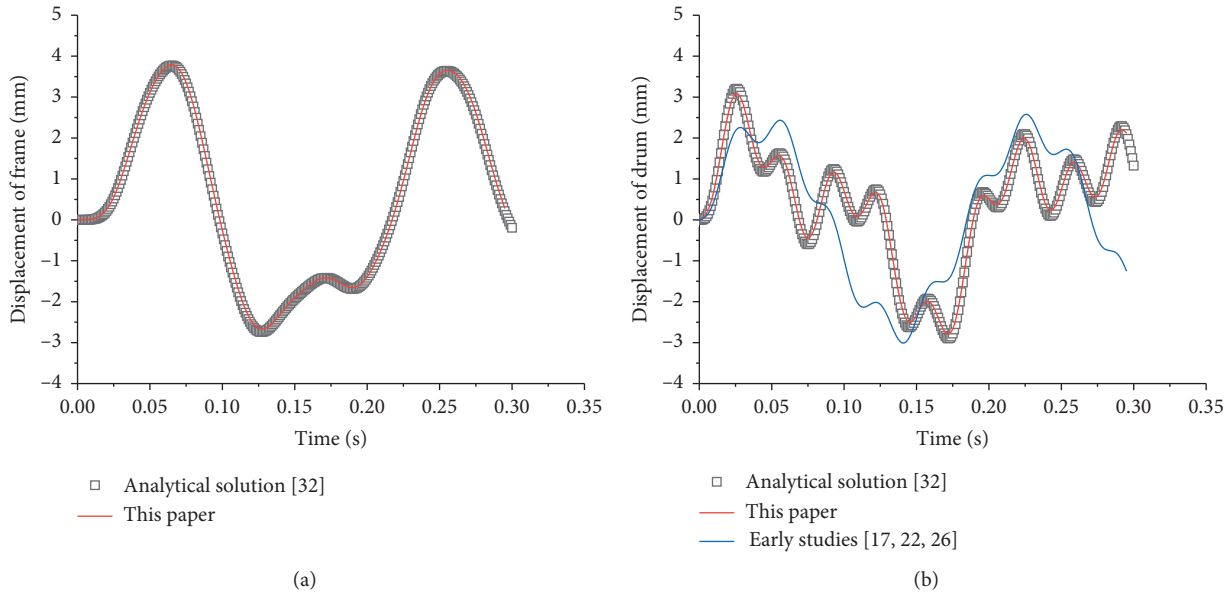

Figure 9: Displacement results of the drum and frame based on numerical simulation and analytical solution. (a) Frame displacement; (b) drum displacement.

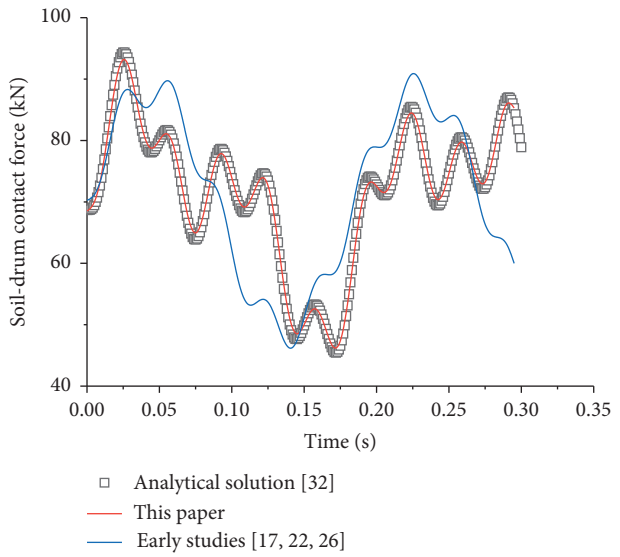

Figure 10: Results of the contact force between the drum and soil.

Table 2: Field experiments of the vibratory roller compaction of field rockfills in the Shui Buya Project.

Rockfill	Quarry blasted limestone
Pavement thickness (mm)	600, 800, 100
Roller type	Tractor-pulled rollers: YZT16, YZT18
Total number of passes	8
Water content (%)	0,10,15,25

Table 3: Properties of the roller YZT16 and YZT18.

Roller type	YZT16	YZT18
Drum mass (kg)	16,000	18,000
Frame mass (kg)	3,000	3,000
Drum width (mm)	2,000	2,000
Drum diameter (mm)	1,800	1,800
Frequency (Hz)	30	27.5
Excitation force magnitude (kN)	354	400
Nominal amplitude (mm)	1.7	1.8
Travel speed (km/h)	2~4	2~4

thicknesses were adopted. A brief introduction of these cases is listed in Table 4.

4.2. DEM Model Calibration-Case A. In this section, numerical investigation on the field rockfill compaction in Case A was performed by the developed discrete method for the purpose of model and parameters calibration.

4.2.1. Discrete Model. Based on the field experiment in Case A, a corresponding discrete model was generated, as illustrated in Figure 12. The numerical model of rockfill pavement is 800 mm in thickness and 6000 mm in width. The thickness of the rockfill pavement model is identical to that of field rockfill pavement, and the width is chosen suitably by experience.

Rockfill particles with different size were generated according to the method introduced in section 2.2. However, it should be noted that the maximum rockfill particle is 800 mm in size, while the smallest is less than 5 mm. The size ratio of the biggest to the smallest particles is as high as 160. Deluzarche [19] has declared that the size ratio should not exceed 10 in a discrete model of rockfill assembly so that the numerical simulation can be accomplished in a reasonable time. Thus, the smaller particles must be avoided. In addition, Zhang [34] has also reported that the effect of the minimum particle on the macroproperties of rockfill

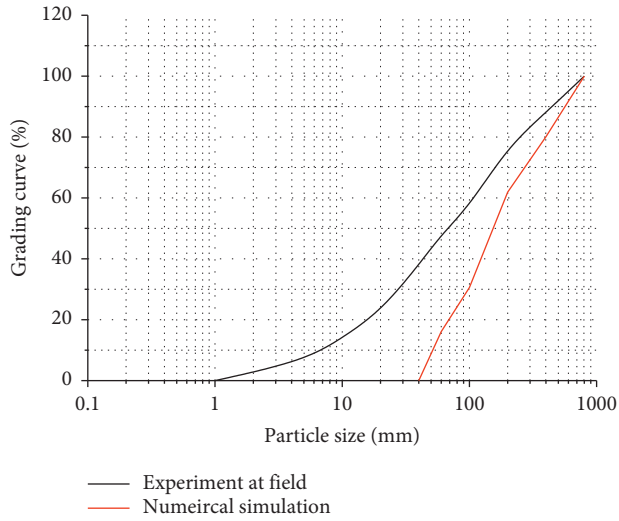

Figure 11: PSDs of field rockfill and numerical rockfill model.

Table 4: Introduction of the three investigated cases.

	Roller type	Thickness of rockfill lift (mm)
Case A	YZT16	800
Case B	YZT18	800
Case C	YZT16	600

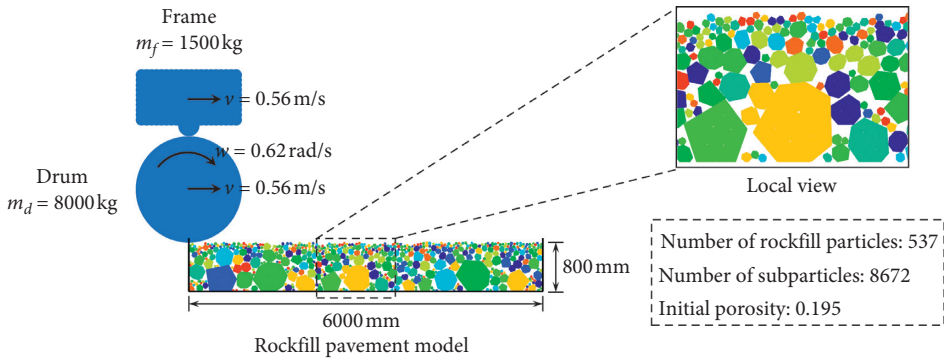

Figure 12: Discrete model of the vibratory roller compaction of field rockfills (Case A).

assembly can be acceptable when the size ratio reaches 4. Thus, the rockfill particles smaller than 40 mm were truncated in this paper, and the size ratio of rockfill particles reached about 20. When the rockfill particles smaller than 40 mm were truncated, the PSD of rockfill pavement model in this paper was a little different from that of field rockfill, as shown in Figure 11.

After the generation procedure, 537 rockfill particles and 8672 subparticles were generated in the rockfill pavement model. The density of the rockfill particle was 2720 kg/m^3. These particles were dropped under gravity with a local friction 0.50, and the initial porosity of the rockfill model was 0.195. The gravity was set to be 9.81 m/s^2.

In this case, the roller YZT16 was modeled. However, the roller YZT16 in the field experiment was 2 m in width, while the roller in simulation was only 1 m (default width in PFC2D). Therefore, the drum and frame mass should be scaled by the ratio of the width of the roller model to that of real roller at field. Thus, the adopted roller parameters in the numerical simulation are listed in Table 5.

During the vibratory roller compaction process, the roller (drum and frame together) moved at a constant horizontal velocity 0.56 m/s, and the drum rotated at a constant angular speed 0.62 rad/s.

4.2.2. Microparameters. The microparameters were calibrated based on the trial and error method. After several trials, the microparameters were determined finally, which were presented in Tables 6–8.

Table 5: Roller Parameters adopted in numerical simulation.

Roller type	YZT16
Drum mass (kg)	8000
Frame mass (kg)	1500
Drum width (mm)	1000 (default in PFC^{2D})
Drum diameter (mm)	1800
Frequency (Hz)	30
Excitation force (N)	177
Nominal amplitude (mm)	1.7
Travel speed (m/s)	0.56

Table 6: Microproperties of PBM contacts between subparticles.

meso parameters		Value
Contact model		Linear parallel bond model
Linear part	Normal stiffness/(N/m)	1.0×10^9
	Shear stiffness/(N/m)	1.0×10^9
	Local friction	0.50
Dashpot part	Normal critical damping ratio	0.20
	Shear critical damping ratio	0.00
	Dashpot mode	3
Bond part	Normal stiffness/(Pa/m)	$1.0\times10^9/(2Rc)$
	Shear stiffness/(Pa/m)	$1.0\times10^9/(2Rc)$
	Tensile strength/(MPa)	2.0
	Shear strength/(MPa)	2.0

where Rc is the size of the bond of PBM contact.

Table 7: Microproperties of linear contacts between rockfill particles.

meso parameters		Value
Contact model		Linear model
Linear part	Normal stiffness (N/m)	1.0×10^9
	Shear stiffness (N/m)	1.0×10^9
	Local friction	0.50
Dashpot part	Normal critical damping ratio	0.20
	Shear critical damping ratio	0.00
	Dashpot mode	3

Table 8: Microparameters of rollers.

Roller type	YZT16	YZT18
Normal stiffness, kn (N/m)	3.70×10^8	3.65×10^8
Normal strength (N)	1×10^{300}	1×10^{300}
Normal critical damping ratio	0.220	0.200
Dashpot mode	3	3

5. Results

5.1. Displacement. After compaction for eight passes, the displacement of rockfill particles is illustrated in Figure 13. It can be found that the displacement distribution of rockfill particles is not uniform, which is caused by the various sizes of the underlying rockfill particles. Besides, the upper half of the rockfill pavement has been compacted sufficiently, while the lower half is not compacted adequately. The results indicate that the influence depth of the vibratory roller is limited, and this is the reason that the rockfill materials are usually paved in thin thickness.

By checking the positions of the rockfill particles located on the top surface, we can obtain the average settlement of the rockfill pavement during the vibratory roller compaction process. However, it is tough for a 2D model to reproduce contracting behavior, just like a 3D one, and the behavior of a 2D sample is thus almost always dilative [19]. Therefore, it is difficult to compare the settlement of the 2D rockfill model to that of the field rockfill directly. So, we have to adopt a relative index, which is termed as relative settlement ratio (RSR), to verify the agreement of numerical simulation and field experiment.

The RSR is defined as follows:

$$\eta_i = \frac{u_{\text{final}} - u_i}{u_{\text{final}}}, \tag{10}$$

where η_i is the RSR of the rockfill pavement in the ith pass, u_{final} is the final settlement after compaction, and u_i is the settlement of the ith pass.

Then, the RSR of the discrete model of the rockfill pavement is compared with that of the field rockfill, which is illustrated in Figure 14. It can be found that the RSR of the numerical simulation agrees well with that of the field experiment. Thus, the numerical model is capable of replicating the settlement of field rockfill under vibratory roller compaction in a qualitative way.

5.2. Breakage of Rockfill Particles. Under vibratory roller compaction, the rockfill particles will suffer severe breakage. Figure 15 illustrates the distribution of cracks, which indicates the breakage of rockfill particles, in the numerical rockfill pavement. Short red lines represent the cracks. According to Figure 15, we can find that the cracks are distributed in the upper half of the rockfill model mostly. Thus, it can be concluded that rockfill particles in the upper half suffer more breakage, while those in the lower half break little.

The breakage of rockfill particles will change the PSD. Thus, the PSDs of the numerical rockfill pavement before and after vibratory roller compaction are analyzed, and the results are illustrated in Figure 16(a). It can be found that numerous small particles (less than 40 mm) are produced, and the content of rockfill particles ranging from 40~60 mm decreases sharply. It indicates that the rockfill particles ranging from 40~60 mm suffer serious breakage during vibratory roller compaction. The reason is that the rockfill particles of 40~60 mm are in the upper half of the rockfill pavement because of segregation, and the magnitude of dynamic stress caused by the vibration roller decreases significantly as the depth increases. As a result, the dynamic stress undertaken by the small particles in the upper half is much higher than that undertaken by the large particles in the lower half.

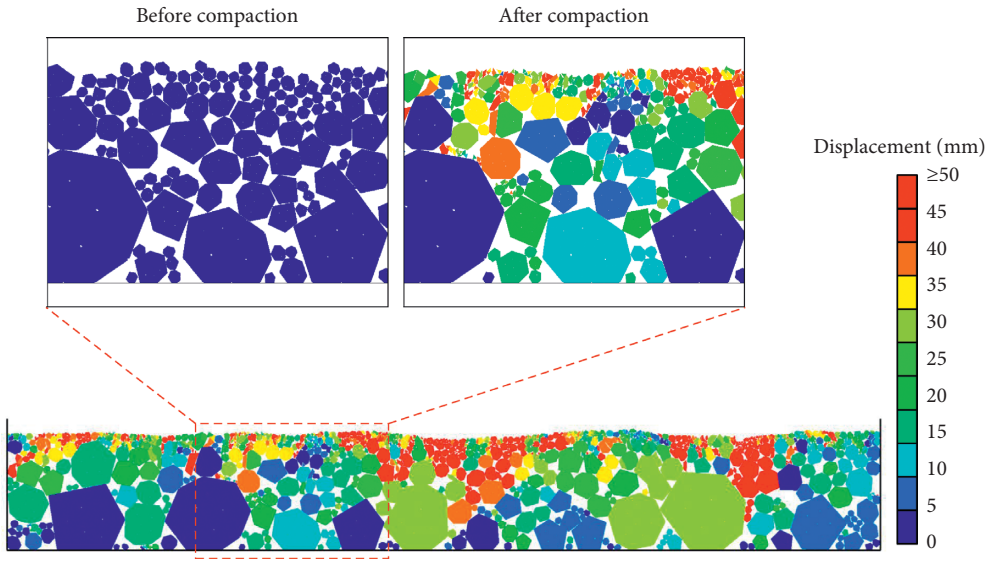

Figure 13: Displacement of rockfill particles after vibratory compaction for eight passes.

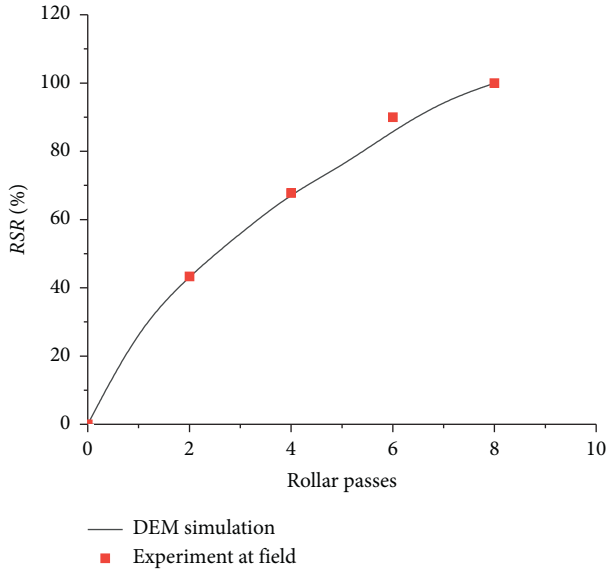

Figure 14: RSR of the rockfill pavement in the verified simulations (Case A).

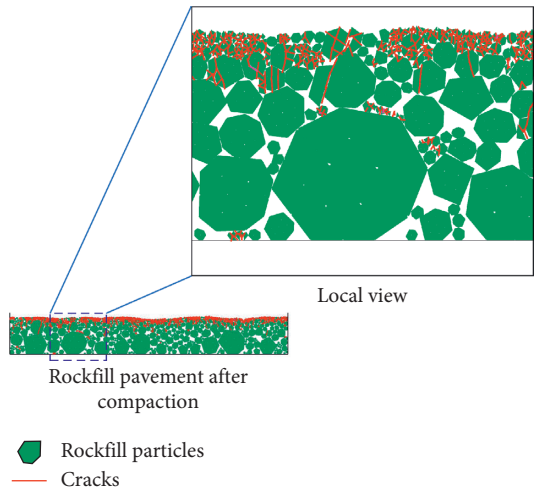

Figure 15: Distribution of cracks in the rockfill model.

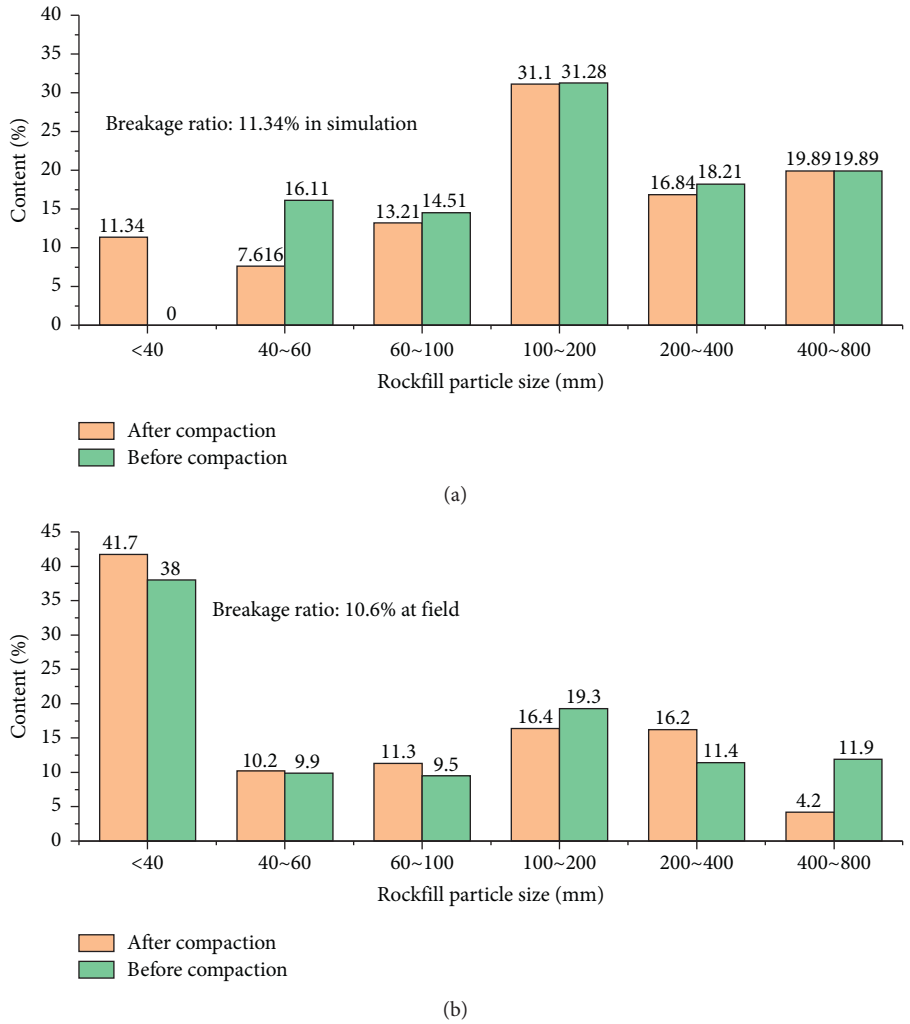

Figure 16: PSD analysis of rockfill particles after compaction at field (16T-800 mm). (a) Numerical simulation; (b) field experiment.

The PSD analysis of rockfill particles at field is also performed, as illustrated in Figure 16(b). According to the PSD analysis, Marsal's breakage ratio of rockfill particles in numerical simulation is 11.34%, and that in the field experiment is 10.6%. Thus, the numerical simulation agrees well with the experiment in situ with the aspect of rockfill particle breakage. However, it should be noted that, in the numerical simulation, particles ranging from 40~60 mm suffer the most severe breakage, while, in the field experiment, particle breakage occurs in the particles ranging from 400~800 mm. The reason for this difference should be related to the fact that the size effect of rockfill particles is not considered in the numerical simulation, of which the crushing strength of large particles is relatively low. Thus, the numerical simulation in this paper is incapable of replicating the PSD evolution of rockfills during vibratory roller compaction yet.

5.3. Porosity. During vibratory roller compaction, the densification of rockfill pavement can be represented by the change of porosity. And it is widely believed that the properties of the upper and lower half of rockfill pavement are different due to particle segregation, and the upper half will experience much more densification. To verify this view, the porosity of the upper and lower half of rockfill pavement is analyzed, respectively.

The rockfill pavement is divided into two layers, the upper and lower half, as illustrated in Figure 17. The thickness of the lower layer is half of the whole pavement, which is constant. As the top surface of the upper half will move down gradually during compaction, the thickness of the upper half is thus not a constant value. In addition, the top surface of the upper half is not a perfect flat surface; thus, the position of the top surface is in fact an average of the vertical positions of the highest points of rockfill particles closest to the top surface.

Note that some rockfill particles go through the boundary between the upper and lower half. For such particles, the proportion of these particles located in the upper half is added to the total area of rockfill particles in the upper half, while the rest of the proportion in the lower half is added to the total area in the lower half.

Then, the porosity of the upper and lower half can be calculated for every compaction pass, respectively, as

Figure 17: Illustration of the upper and lower half of rockfill pavement.

shown in Figure 18. It can be found that the porosities of the upper and lower half both decrease as the compaction pass increases. However, the porosity of the upper half decreases evidently, while that of the lower half changes only a little. It proves that rockfill particles in the upper half are compacted sufficiently, while those in the lower half are not.

It should be also noted that the porosity of the upper half is always larger than that of the lower half. However, this may be not true as field experiments have revealed that the density of the upper half is larger than that of the lower half [5]. The reason may be that small particles smaller than 40 mm, which mainly locate in the upper half and fill the voids of rockfill particles, are truncated in the numerical simulation. Thus, the porosity of the upper half may be overestimated.

5.4. DEM Model Prediction: Cases B and C. Based on the numerical model and calibrated microparameters, the vibratory roller compaction of field rockfill in cases B and C was also simulated. These performed numerical simulations can be regarded as prediction of the dynamic response of rockfill pavement. Moreover, the predicted results are compared with those from the experiments in situ.

The RSRs of the rockfill models in cases B and C, compared with the results of field experiments, are presented in Figure 19. It is also evident that the numerical results in cases B and C agree well with those of the field experiments. Thus, we can conclude that the proposed numerical model can predict the settlement of field rockfills reasonably.

Similarly, the PSDs of rockfill pavement in cases B and C are also analyzed, and the results are illustrated in Figure 20. According to the results of case B, the breakage ratio of rockfill in simulation is 13.02%, while the breakage ratio measured at field is 9.3%. In case C, the breakage ratio of rockfill in simulation is 13.7%; however, the breakage ratio of rockfill at field is not available. Thus, they are not compared. In addition, rockfill particles ranging from 40~60 mm suffer the most serious breakage in simulation, while breakage mainly occurs in the rockfill particles ranging from 400~800 mm in the field experiments. And the reason has been explained above.

The porosity evolution of rockfill model during vibratory roller compaction is illustrated in Figure 21. And the porosity of the upper and lower half is analyzed, respectively. It can be also found that the porosity of the upper half decreases significantly, while that of the lower half changes

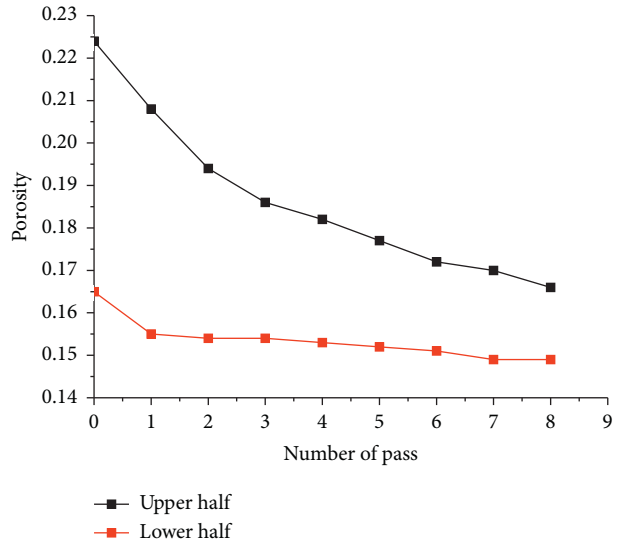

Figure 18: Porosity of the upper and lower half during vibratory roller compaction.

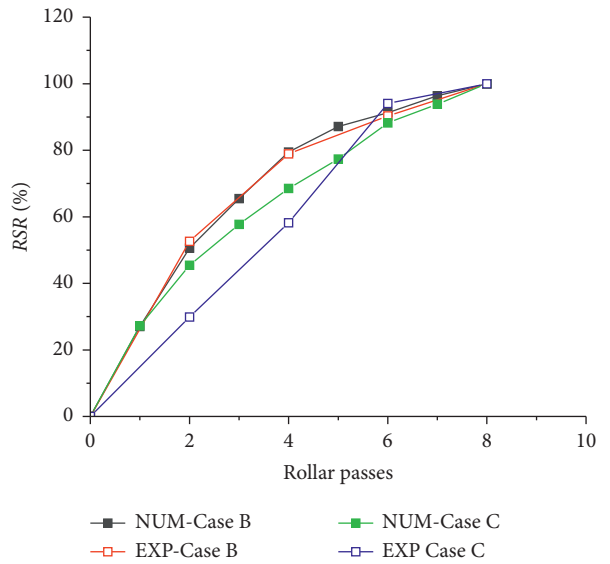

Figure 19: RSRs of the rockfill pavements in case B and case C.

only a little in both cases B and C, which proves the fact that rockfill particles in the upper half of pavement are easier to be compacted.

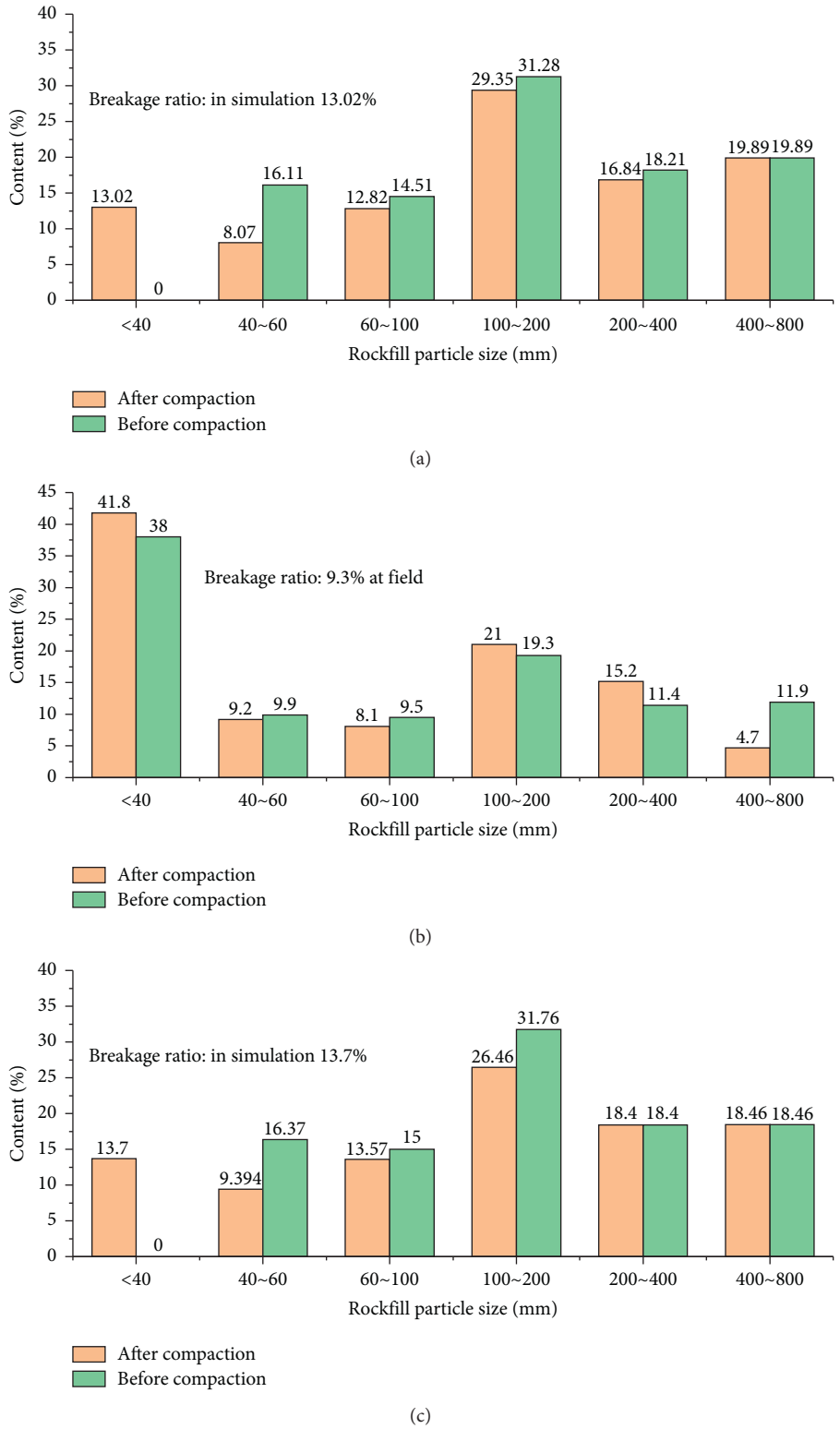

Figure 20: PSD analysis of rockfill particles in case B and case C. (a) Case B NUM. (b) Case B EXP. (c) Case C NUM.

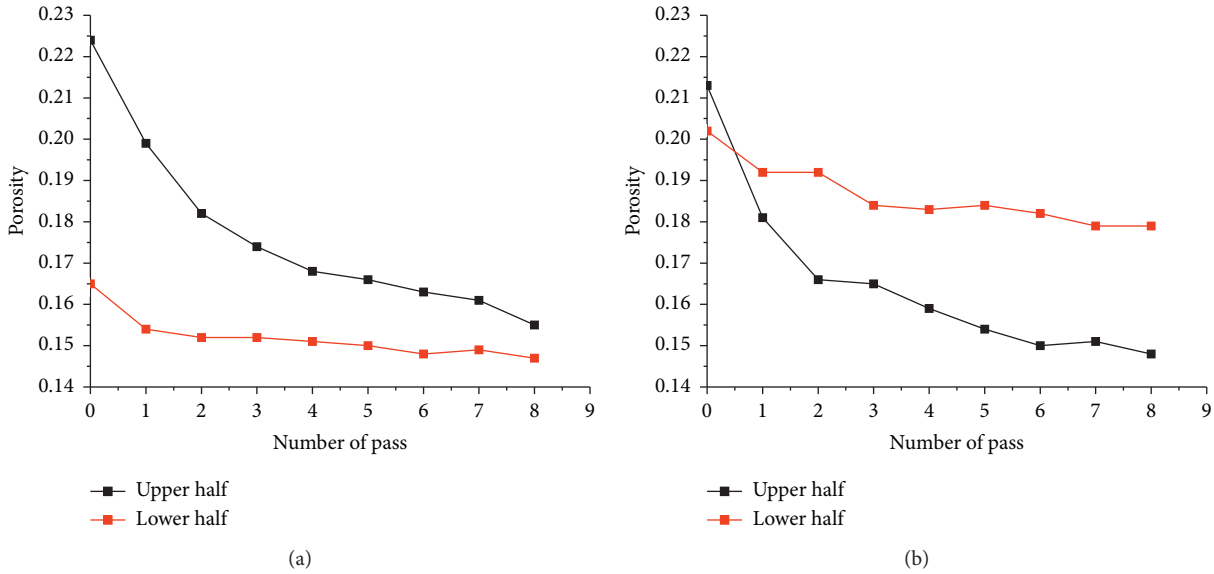

Figure 21: Porosity evolution of the upper and lower half of the rockfill model during compaction. (a) Case B. (b) Case C.

6. Conclusion

In this paper, a numerical simulation of vibratory roller compaction of field rockfills was performed based on the discrete element method. Especially, we have presented a new numerical model of the vibratory roller with the frame inertia considered, which overcomes the disadvantage of the roller models in early studies. The following conclusions are obtained:

(1) Vibratory roller compaction of field rockfills can be simulated with the developed discrete simulation method reasonably. In addition, the feasibility and rationality of the developed simulation method are proved.

(2) Based on calibrated model and parameters, the displacement, breakage, PSD, and porosity evolution of field rockfills under vibratory roller compaction with various roller parameters can be predicted well, which indicates the prospect of the developed numerical method in application of engineering.

(3) The new roller model, in which the frame inertia is considered, is much more accurate than those in early studies, in which only the drum is modeled.

Data Availability

The data used to support the findings of this study are included within the article and are available from the corresponding author upon request.

Conflicts of Interest

The authors declare no conflicts of interest.

References

[1] H. Ma and F. Chi, "Major technologies for safe construction of high earth-rockfill dams," *Engineering*, vol. 2, no. 4, pp. 498–509, 2016.

[2] H. Ma and F. Chi, "Technical progress on researches for the safety of high concrete-faced rockfill dams," *Engineering*, vol. 2, no. 3, pp. 332–339, 2016.

[3] L. Wen, J. Chai, Z. Xu, Y. Qin, and Y. Li, "A statistical review of the behaviour of concrete-face rockfill dams based on case histories," *Géotechnique*, vol. 68, no. 9, pp. 749–771, 2018.

[4] B. Xu, D. Zou, X. Kong, Z. Hu, and Y. Zhou, "Dynamic damage evaluation on the slabs of the concrete faced rockfill dam with the plastic-damage model," *Computers and Geotechnics*, vol. 65, pp. 258–265, 2015.

[5] J. B. Cooke, "Progress in rockfill dams," *Journal of Geotechnical Engineering*, vol. 110, no. 10, pp. 1381–1414, 1984.

[6] D. Zhong, D. Liu, and B. Cui, "Real-time compaction quality monitoring of high core rockfill dam," *Science China Technological Sciences*, vol. 54, no. 7, pp. 1906–1913, 2011.

[7] S. Zhu, C. Zhong, J. Wang et al., "Experimental study on filling standard of high rockfill dams with soil core," *Chinese Journal of Geotechnical Engineering*, vol. 41, no. 3, pp. 561–566, 2019, [in Chinese].

[8] S. Zhu, "Study and application of control indices for filling quality of high concrete face rockfill dams," *Chinese Journal of Geotechnical Engineering*, vol. 42, no. 4, pp. 610–615, 2020, [in Chinese].

[9] Z. An, T. Liu, Z. Zhang, Q. Zhang, Z. Huangfu, and Q. Li, "Dynamic optimization of compaction process for rockfill materials," *Automation in Construction*, vol. 110, Article ID 103038, 2020.

[10] M. A. Mooney and R. V. Rinehart, "In situ soil response to vibratory loading and its relationship to roller-measured soil stiffness," *Journal of Geotechnical and Geoenvironmental Engineering*, vol. 135, no. 8, pp. 1022–1031, 2009.

[11] R. V. Rinehart and M. A. Mooney, "Measurement depth of vibratory roller-measured soil stiffness," *Géotechnique*, vol. 59, no. 7, pp. 609–619, 2009.

[12] M. A. Mooney and R. V. Rinehart, "Field monitoring of roller vibration during compaction of subgrade soil," *Journal of Geotechnical and Geoenvironmental Engineering*, vol. 133, no. 3, pp. 257–265, 2007.

[13] H.-C. Dan, D. Yang, X. Liu, A.-P. Peng, and Z. Zhang, "Experimental investigation on dynamic response of asphalt

pavement using smartrock sensor under vibrating compaction loading," *Construction and Building Materials*, vol. 247, Article ID 118592, 2020.

[14] C. Wersäll, I. Nordfelt, and S. Larsson, "Soil compaction by vibratory roller with variable frequency," *Géotechnique*, vol. 67, no. 3, pp. 272–278, 2017.

[15] C. Wersäll, I. Nordfelt, and S. Larsson, "Resonant roller compaction of gravel in full-scale tests," *Transportation Geotechnics*, vol. 14, pp. 93–97, 2018.

[16] D. Liu, Z. Li, and J. Liu, "Experimental study on real-time control of roller compacted concrete dam compaction quality using unit compaction energy indices," *Construction and Building Materials*, vol. 96, pp. 567–575, 2015.

[17] B. Kenneally, O. M. Musimbi, J. Wang, and M. A. Mooney, "Finite element analysis of vibratory roller response on layered soil systems," *Computers and Geotechnics*, vol. 67, pp. 73–82, 2015.

[18] P. A. Cundall and O. D. L. Strack, "A discrete numerical model for granular assemblies," *Géotechnique*, vol. 29, no. 1, pp. 47–65, 1979.

[19] R. Deluzarche and B. Cambou, "Discrete numerical modelling of rockfill dams," *International Journal for Numerical and Analytical Methods in Geomechanics*, vol. 30, no. 11, pp. 1075–1096, 2006.

[20] E. Alaei and A. Mahboubi, "A discrete model for simulating shear strength and deformation behaviour of rockfill material, considering the particle breakage phenomenon," *Granular Matter*, vol. 14, no. 6, pp. 707–717, 2012.

[21] F. Yao, G. Ma, S. Guan, Y. Chen, Q. Liu, and C. Feng, "Interfacial shearing behavior analysis of rockfill using FDEM simulation with irregularly shaped particles," *International Journal of Geomechanics*, vol. 20, no. 3, Article ID 04019193, 2020.

[22] D. Liu, L. Sun, H. Ma, and W. Cui, "Process simulation and mesoscopic analysis of rockfill dam compaction using discrete element method," *International Journal of Geomechanics*, vol. 20, no. 6, Article ID 04020047, 2020.

[23] Y. Jia, B. Xu, S. Chi, B. Xiang, D. Xiao, and Y. Zhou, "Particle breakage of rockfill material during triaxial tests under complex stress paths," *International Journal of Geomechanics*, vol. 19, no. 12, Article ID 04019124, 2019.

[24] Y. Liu, X. Li, and S. Wu, "Numerical simulation of particle crushing for rockfill of different particles shape under rolling compaction," *Rock and Soil Mechanics*, vol. 35, no. 11, pp. 3269–3280, 2014, [in Chinese].

[25] Li Yang, c.-x. She, and X.-l. Jiao, "A new method for simulating rockfill roller compaction using particle flow code," *Rock and Soil Mechanics*, vol. 38, no. 10, pp. 3029–3038, 2017, [in Chinese].

[26] I. Paulmichl, T. Furtmüller, C. Adam, and D. Adam, "Numerical simulation of the compaction effect and the dynamic response of an oscillation roller based on a hypoplastic soil model," *Soil Dynamics and Earthquake Engineering*, vol. 132, Article ID 106057, 2020.

[27] Itasca Consulting Group, *Particle Flow Code: SoftWare Manual*, ITASCA, Minneapolis, MI, USA, 2018.

[28] G. Ma, W. Zhou, and X.-L. Chang, "Modeling the particle breakage of rockfill materials with the cohesive crack model," *Computers and Geotechnics*, vol. 61, pp. 132–143, 2014.

[29] W. Zhou, L. Yang, G. Ma et al., "DEM modeling of shear bands in crushable and irregularly shaped granular materials," *Granular Matter*, vol. 19, no. 2, pp. 1–12, 2017.

[30] Z. Nie, Y. Zhu, X. Wang et al., "Investigating the effects of Fourier-based particle shape on the shear behaviors of rockfill material via DEM," *Granular Matter*, vol. 21, no. 2, 2019.

[31] M. Zhou and E. Song, "A random virtual crack DEM model for creep behavior of rockfill based on the subcritical crack propagation theory," *Acta Geotechnica*, vol. 11, no. 4, pp. 827–847, 2016.

[32] T. S. Yoo and E. T. Selig, "Dynamics OF vibratory-roller compaction," *Journal of the Geotechnical Engineering Division-Asce*, vol. 105, no. 10, pp. 1211–1231, 1979.

[33] L. Changcai, *Research on the Key Technology Applied in the Construction of the Shui Buya Rockfill Dam*, China Water-Power Press, Bei Jing, China, [in Chinese], 2005.

[34] Y. Zhang, W. Zhou, G. Ma et al., "Effect of minimum particle size on mechanical properties of rockfill materials by numerical simulation," *Engineering Journal of Wuhen Universiy*, vol. 50, no. 3, pp. 332–339, 2017, [in Chinese].